Studies of nuclear pear-shapes using accelerated radioactive beams

Published: 9th May 2013 | Vol 497 | Nature | p199 | doi:10.1038/nature12073

L.P. Gaffney[1], P.A. Butler[1], M. Scheck[1,2], A.B. Hayes[3], F. Wenander[4], M. Albers[5], B. Bastin[6], C. Bauer[2], A. Blazhev[5], S. Bönig[2], N. Bree[7], J. Cederkäll[8], T. Chupp[9], D. Cline[3], T.E. Cocolios[4], T. Davinson[10], H. De Witte[7], J. Diriken[7,11], T. Grahn[12], A. Herzan[12], M. Huyse[7], D.G. Jenkins[13], D.T. Joss[1], N. Kesteloot[7,11], J. Konki[12], M. Kowalczyk[14], Th. Kröll[2], E. Kwan[15], R. Lutter[16], K. Moschner[5], P. Napiorkowski[14], J. Pakarinen[4,12], M. Pfeiffer[5], D. Radeck[5], P. Reiter[5], K. Reynders[7], S.V. Rigby[1], L.M. Robledo[17], M. Rudigier[5], S. Sambi[7], M. Seidlitz[5], B. Siebeck[5], T. Stora[4], P. Thoele[5], P. Van Duppen[7], M. Vermeulen[13], M. von Schmid[2], D. Voulot[4], N. Warr[5], K. Wimmer[18], K. Wrzosek-Lipska[7], C.Y. Wu[15], & M. Zielinska[14]

There is strong circumstantial evidence that the shape of atomic nuclei with particular values of *Z* and *N* prefers to assume octupole deformation, in which the nucleus is distorted into a pear shape that loses the reflection symmetry of a quadrupole-deformed (rugby ball) shape prevalent in nuclei. Recently, useable intensities of accelerated beams of heavy, radioactive ions have become available at the REX-ISOLDE facility at CERN. This has allowed electric octupole transition strengths, a direct measure of octupole correlations, to be determined for short-lived isotopes of radon and radium expected to be unstable to pear-like distortions. The data are used to discriminate differing theoretical approaches to the description of the octupole phenomena, and also help restrict the choice of candidates for studies of atomic electric-dipole moments, that provide stringent tests of extensions to the Standard Model.

[1]University of Liverpool, UK. [2] Technische Universität Darmstadt, Germany. [3]University of Rochester, USA. [4]CERN-ISOLDE. [5] Universität zu Köln, Germany. [6]GANIL, France. [7]KU Leuven, Belgium. [8]University of Lund, Sweden. [9]University of Michigan, USA. [10]University of Edinburgh, UK. [11]SCK CEN, Belgium. [12]University of Jyväskylä, and Helsinki Institute of Physics, Finland. [13]University of York, UK. [14]University of Warsaw, Heavy Ion Laboratory, Poland. [15]Lawrence Livermore National Laboratory, USA. [16]Ludwig-Maximilians-Universität München, Germany. [17]Universidad Autónoma de Madrid, Spain. [18]Technische Universität München, Germany.

The atomic nucleus is a many-body quantum system and hence its shape is determined by the number of nucleons present in the nucleus and the interactions between them. For example, nuclei in their ground state in which the proton and neutron shells are completely filled ("doubly magic" nuclei) are spherical. If this configuration is excited, or if more nucleons are added, the long-range correlations between valence nucleons distort the shape from spherical symmetry and the nucleus becomes deformed. In most of these cases, it is well established that the shape assumed has quadrupole deformation with axial and reflection symmetry, i.e. shaped
like a rugby ball (prolate deformation) or as a flattened spheroid (oblate deformation). For certain combinations of protons and neutrons there is also the theoretical expectation that the shape of nuclei can assume octupole deformation, corresponding to reflection asymmetry or a "pear-shape" in the intrinsic frame, either dynamically (octupole vibrations) or statically (permanent octupole deformation).

Atoms with octupole-deformed nuclei are very important in the search for permanent atomic electric-dipole moments (EDMs). The observation of a non-zero EDM at the level of contemporary experimental sensitivity would indicate time-reversal (T) or equivalently charge-parity (CP) violation due to physics beyond the Standard Model. In fact, experimental limits on EDMs provide important constraints on many proposed extensions to the Standard Model[1,2]. For a neutral atom in its ground state, the Schiff moment, the electric dipole distribution weighted by radius squared[3], is the lowest order observable nuclear moment. Octupole-deformed odd-A nuclei will have enhanced nuclear Schiff moments due to the presence of the large octupole collectivity and the occurrence of nearly degenerate parity doublets that naturally arise if the deformation is static[3,4,5]. Since a CP-violating Schiff moment induces a contribution to the atomic EDM, the sensitivity over non-octupole-enhanced systems such as ^{199}Hg [2], currently providing the most stringent limit for atoms, can be improved by a factor of 100-1000 [4]. Essential in the interpretation of such limits in terms of new physics is a detailed understanding of the structure of these nuclei. Experimental programmes are in

place to measure EDMs in atoms of odd-mass Rn and Ra isotopes in the octupole region (see e.g. ref. 6) but so far there is little direct information on octupole correlations in these nuclei.

Strong octupole correlations leading to pear shapes can arise when nucleons near the Fermi surface occupy states of opposite parity with orbital and total angular momentum differing by $3\hbar$. This condition is met for proton number $Z\sim$ 34, 56, and 88 and neutron number $N\sim$ 34, 56, 88, and 134. The largest array of evidence for reflection asymmetry is seen at the values of $Z\sim$88 and $N\sim$134, where phenomena such as interleaved positive- and negative-parity rotational bands in even-even nuclei[7], parity doublets in odd-mass nuclei[8], and enhanced electric-dipole ($E1$) transition moments[9] have been observed. Many theoretical approaches have been developed to describe the observed experimental features: shell-corrected liquid-drop models[10,11], mean-field approaches using various interactions[12,13,14,15,16], models that assume α-particle clustering in the nucleus[17,18], algebraic models[19], and other semi-phenomenological approaches[20]. A broad overview of the experimental and theoretical evidence for octupole correlations is given in ref. 21.

In order to determine the shape of nuclei, the rotational model can be employed to connect the intrinsic deformation, which is not directly observable, to the electric charge moments that arise from the non-spherical charge distribution. For quadrupole deformed nuclei the typical experimental observables are the electric-quadrupole ($E2$) transition moments that are related to the matrix elements connecting differing members of rotational bands in these nuclei, and $E2$ static moments that are related to diagonal matrix elements for a single state. If the nucleus does not change its shape under rotations, both types of moments will vary with angular momentum but can be related to a constant "intrinsic" moment that characterises the shape of the nucleus. For pear-shaped nuclei there will be additionally $E1$ and electric-octupole ($E3$) transition moments that connect rotational states having opposite parity. The $E1$ transitions can be enhanced because of the separation of the centre-of-mass and centre-of-charge. The absolute values of the $E1$ moments are, however, small ($< 10^{-2}$ single particle units) and are dominated by single-particle and cancellation effects[9]. In contrast

the $E3$ transition moment is collective in behaviour (> 10 single particle units) and is quite insensitive to single-particle effects, as it is generated by coherent contributions arising from the quadrupole-octupole shape. The $E3$ moment is therefore an observable that should provide direct evidence for enhanced octupole correlations and, for deformed nuclei, can be related to the intrinsic octupole deformation parameters[22]. Until the present measurements, $E3$ transition strengths have been determined for only one nucleus in the $Z\sim 88$, $N\sim134$ region, ^{226}Ra [23], so that theoretical calculations of $E3$ moments in reflection-asymmetric nuclei have not yet been subject to detailed scrutiny.

Coulomb excitation (Coulex) is an important tool for exploring the collective behaviour of deformed nuclei that gives rise to strong enhancement of the probability of transitions between excited states. Traditionally, this technique has been employed by exciting targets of stable nuclei with accelerated ion beams of stable nuclei at energies below the Coulomb barrier to ensure that the interaction is purely electromagnetic in character. Whereas $E2$ and $E1$ (and magnetic dipole $M1$) transition probabilities dominate in the electromagnetic decay of nuclear states, and hence can be determined from measurements of the lifetimes of the states, $E2$ and $E3$ transition strengths dominate the Coulomb excitation process allowing these strengths to be determined from measurement of the cross-sections of the states, often inferred from the γ-rays seen to de-excite these levels. In exceptional cases, the Coulex technique has been applied to radioactive targets like ^{226}Ra which is sufficiently long-lived (half-life of 1600 yrs) to produce a macroscopic sample. It is only comparatively recently that the technique has been extended to the use of accelerated beams of radioactive nuclei such as those from the REX-ISOLDE[24] facility at CERN. In the experiments described here ^{220}Rn (Z=86, N=134) and ^{224}Ra (Z=88, N=136) ions were produced by spallation in a thick UC_x target bombarded by $\sim10^{13}$ proton/s at 1.4 GeV from the CERN PS Booster. The ions were post-accelerated in REX-ISOLDE to an energy of 2.82 or 2.83 A-MeV and bombarded secondary targets of ^{60}Ni, ^{114}Cd and ^{120}Sn of thickness ~ 2 mg/cm^2 with an intensity of about 3×10^5 ions/s and 7×10^5 ions/s for respectively, Rn and Ra, (see "Methods"). The targets were chosen to give

differing electromagnetic excitation (Ni, Z=28 versus Sn, Z=50; see figure 1) and in the case of ^{114}Cd, to provide a cross-check to the excitation of a target whose matrix elements are well known.

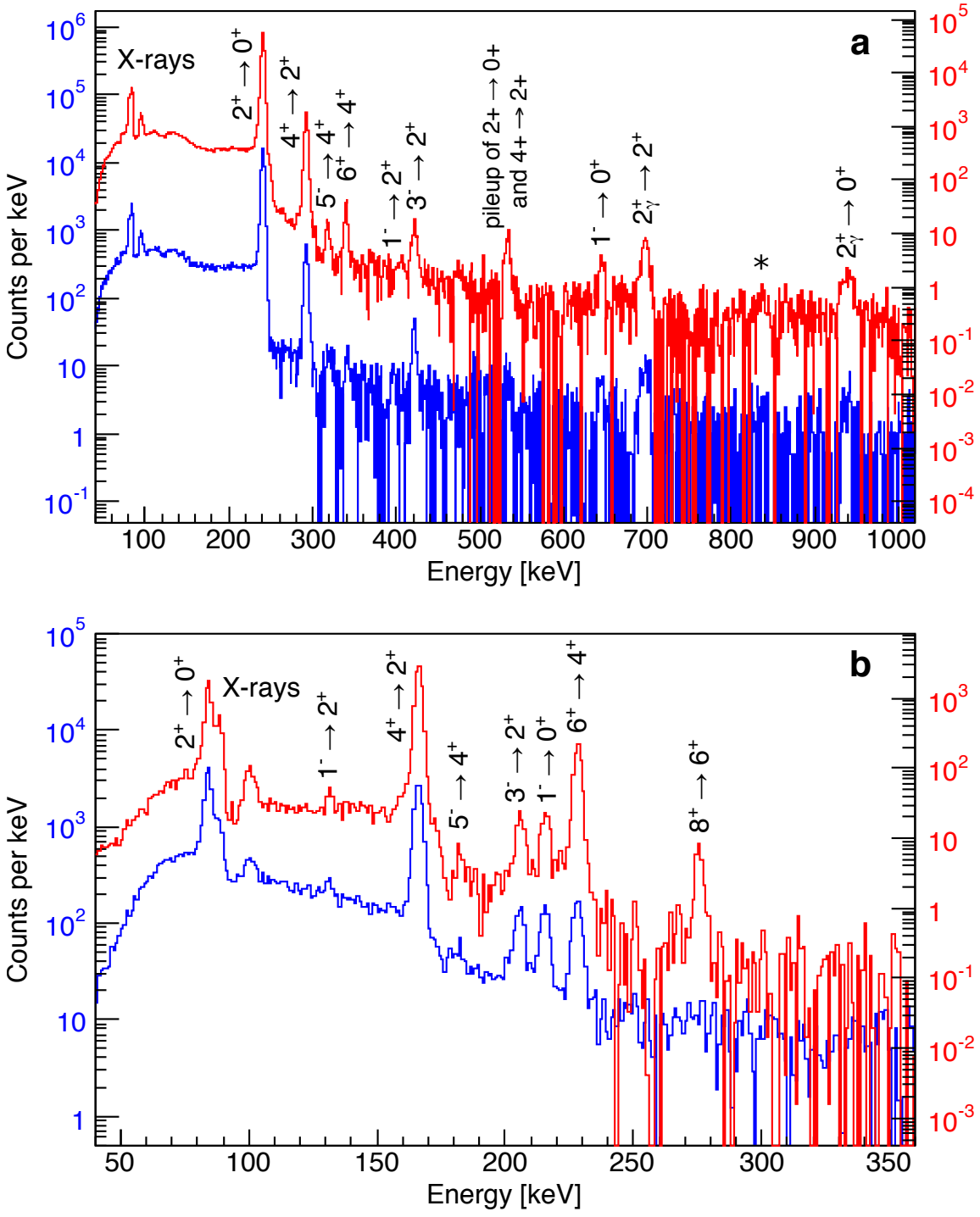

Figure 1. Representative γ-ray spectra following the bombardment of a 2mg/cm^2 ^{60}Ni (blue) and ^{120}Sn (red) targets by (a) ^{220}Rn and (b) ^{224}Ra. The differences in excitation cross-section for the different Z targets are apparent for the higher spin states. The γ rays are corrected for Doppler shift assuming that they are emitted from the scattered projectile. The asterisk in (a) marks an unassigned, 836(2) keV transition. A state at 937.8(8) keV is assigned $I^{\pi} = 2^+$ on the basis of its excitation and decay properties; it is assumed to be the bandhead of the γ-band in ^{220}Rn.

The γ-rays emitted following the excitation of the target and projectile nuclei were detected in MINIBALL[25], an array of 24 high-purity germanium detectors, each with six-fold segmentation and arranged in 8 triple-clusters. The scattered projectiles and target recoils, distinguished by their differing dependence of energy with laboratory angle, were detected in a highly-segmented silicon detector[26]. Representative spectra for ^{220}Rn and ^{224}Ra, for which the γ-ray energy is corrected for Doppler shift assuming emission from the scattered projectile, are shown in figure 1. Here events were accumulated only if the target recoil was detected in coincidence with γ-rays within a 600 ns time window; these were corrected for random events. The energy level schemes for ^{220}Rn and ^{224}Ra are shown in figure 2.

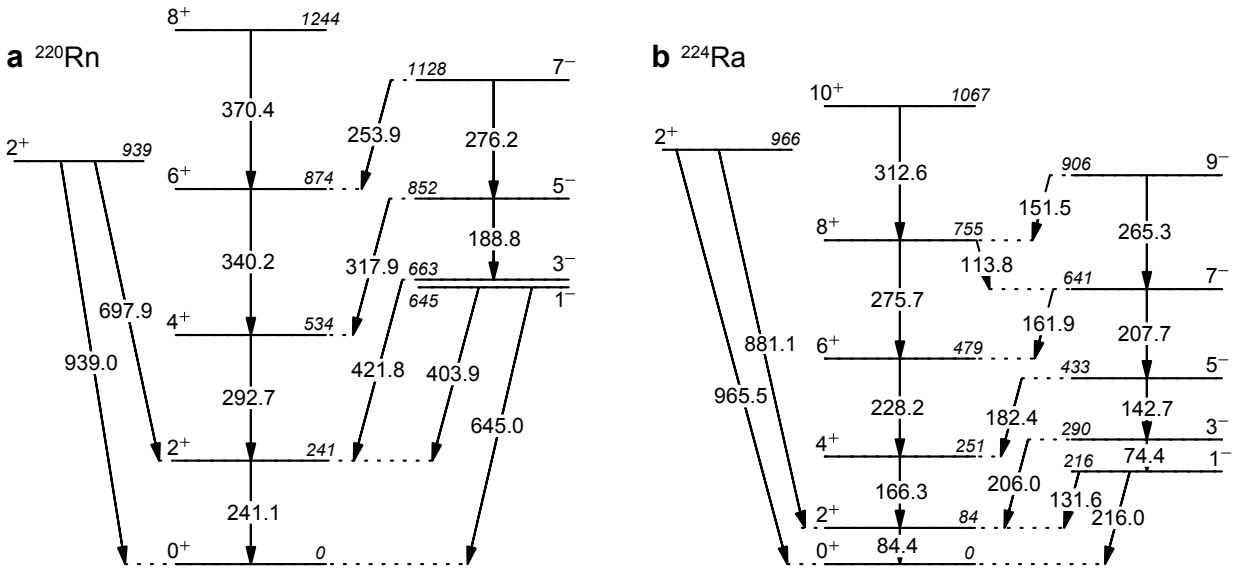

Figure 2: Partial level-schemes for ^{220}Rn (a) and ^{224}Ra (b) showing the excited states of interest for this work. Arrows indicate known γ-ray transitions. All energies are in keV and spins in units of $\hbar$. Note that the level at 939 keV in ^{220}Rn is observed for the first time in this work.

The spectra reveal strong population of the ground state band of positive-parity states, excited by direct and multiple *E*2 Coulomb excitation, and substantial population of the octupole band of negative-parity states, excited by *E*3 excitation. The yields of the observed γ-ray transitions detected in MINIBALL were measured for two ranges of the recoil angle of the target nucleus (28-38°, 38-52° for ^{220}Rn and 24-40°, 40-54° for ^{224}Ra) for each of the three targets, and combined with existing spectroscopic data (lifetimes of low-lying states[27,28] and their γ-ray branching ratios[7,29,30]) to provide

input to the Coulomb-excitation analysis code GOSIA[31] (see "Methods"). The separation of angular ranges increased sensitivity in the measurement by varying the relative excitation probabilities. For ^{220}Rn, 34 independent data determined 22 free parameters (16 matrix elements and 1 normalisation constant for each combination of target and recoil angle range) while for ^{224}Ra, 57 data determined 23 free parameters (17 matrix elements). The analysis was also carried out for ^{220}Rn independently of the previously measured lifetime of the 2^+ state (τ_{2+}) [27], and for ^{224}Ra independently of τ_{4+} [28]. (In the latter case the previously measured value of τ_{2+} cannot be determined independently as the $2^+ \rightarrow 0^+$ transition is contaminated with the Ra X-rays.) In both cases the fitted matrix elements for the $2^+ \rightarrow 0^+$ $E2$ transition (^{220}Rn) and for the $4^+ \rightarrow 2^+$ $E2$ transition (^{224}Ra) were found to agree, within the experimental uncertainties, with the values obtained using the lifetime measurements.

The measured $E1$, $E2$ and $E3$ matrix elements for ^{220}Rn and ^{224}Ra are given in table 1. The values of the intrinsic moments, Q_λ, are given in figure 3. These are determined from the experimental values of $\langle I||E\lambda||I'\rangle$ assuming the validity of the rotational model[22]. For the $E2$ and $E3$ matrix elements the measured values are all consistent with the geometric predictions expected from a rotating, deformed distribution of electric charge, although these data do not distinguish whether the negative-parity states arise from the projection of a quadrupole-octupole deformed shape or from an octupole oscillation of a quadrupole shape[32]. Table 2 compares the experimental values of Q_λ derived from the matrix elements connecting the lowest states for nuclei near Z=88 and N=134 measured by Coulomb excitation. It is striking that while the $E2$ moment increases by a factor of 6 between ^{208}Pb and ^{234}U, the $E3$ moment changes by only 50% in the entire mass region. Nevertheless the larger Q_3 values for ^{224}Ra and ^{226}Ra indicate an enhancement in octupole collectivity that is consistent with an onset of octupole deformation in this mass region. On the other hand ^{220}Rn has similar octupole strength to ^{208}Pb, ^{230,232}Th, and ^{234}U, consistent with it being an octupole vibrator. In the case of a vibrator the coupling of an octupole phonon to the ground state rotational band will give zero values for matrix elements such as $\langle 1^-||E3||4^+\rangle$, since an aligned octupole phonon would couple the 4^+ state to a 7^- state. Although the present experiment does not have sensitivity to this quantity, this effect has

been observed for ^{148}Nd in the Z~56, N~88 octupole region[38], while for ^{226}Ra the intrinsic moment derived from the measured $<1^-||E3||4^+>$ is similar to that derived from the value of $<0^+||E3||3^->$ [23]. The deduced shapes of ^{220}Rn and ^{224}Ra are presented in figure 4. Here the values of quadrupole and octupole deformation β_2 and β_3 were extracted from the dependence of the measured Q_2 and Q_3 on the generalised nuclear shape[39].

Table 1. Values of matrix elements measured in the present experiment. The uncertainties include the 1σ statistical error from the fit (χ^2+1 type) and systematic contributions – beam energy and target thickness uncertainties, deorientation, beam spot effects etc. The values of B(Eλ) for electromagnetic decay are derived from the matrix elements and are given in single particle units ("Weisskopf" units or Wu) . The upper limits correspond to 3σ.

matrix element $<I\|\|E\lambda\|\|I'>$	^{220}Rn |m.e.| (efm$^\lambda$)	^{220}Rn $B(E\lambda)\downarrow$ (Wu)	^{224}Ra |m.e.| (efm$^\lambda$)	^{224}Ra $B(E\lambda)\downarrow$ (Wu)
$<0^+\|\|E1\|\|1^->$	< 0.10	$< 1.5 \times 10^{-3}$	< 0.018	$< 5 \times 10^{-5}$
$<2^+\|\|E1\|\|1^->$	< 0.13	$< 3 \times 10^{-3}$	< 0.03	$< 1.3 \times 10^{-4}$
$<2^+\|\|E1\|\|3^->$	< 0.18	$< 2 \times 10^{-3}$	0.026±0.005	$3.9^{+1.7}_{-1.4} \times 10^{-5}$
$<4^+\|\|E1\|\|5^->$	0.028±0.009	$3.0^{+2}_{-1.6} \times 10^{-5}$	0.030±0.010	$4^{+3}_{-2} \times 10^{-5}$
$<6^+\|\|E1\|\|7^->$	< 1.3	< 0.5	< 0.10	$< 3 \times 10^{-4}$
$<0^+\|\|E2\|\|2^+>$	137±4	48±3	199±3	98±3
$<1^-\|\|E2\|\|3^->$	180±60	60^{+50}_{-30}	230±11	93±9
$<2^+\|\|E2\|\|4^+>$	212±4	63±3	315±6	137±5
$<3^-\|\|E2\|\|5^->$	220±150	60^{+100}_{-50}	410±60	190±60
$<4^+\|\|E2\|\|6^+>$	274±14	73±8	405±15	156±12
$<6^+\|\|E2\|\|8^+>$			500±60	180±60
$<0^+\|\|E2\|\|2^+_\gamma>$	32±7	2.6±1.1	23±4	1.3±0.5
$<0^+\|\|E3\|\|3^->$	810±50	33±4	940±30	42±3
$<2^+\|\|E3\|\|1^->$	< 2600	< 760	1370±140	210±40
$<2^+\|\|E3\|\|3^->$	< 5300	< 1400	< 4000	< 600
$<2^+\|\|E3\|\|5^->$	1700±400	90±50	1410±190	61±17

Table 2. The values of the $E2$ and $E3$ intrinsic moments, Q_λ, derived from the matrix elements (see caption to figure 3) connecting the lowest-lying states in nuclei near Z=88 and N=134. The values for ^{220}Rn and ^{224}Ra are taken from the present work.

nucleus	^{208}Pb	^{220}Rn	^{224}Ra	^{226}Ra	^{230}Th	^{232}Th	^{234}U
Q_2 (efm^2)	179±4[33]	434±14	632±10	717±3[23]	900±6[34]	932±5[36]	1047±5[34]
Q_3 (efm^3)	2100±20[33]	2180±130	2520±90	2890±80[23]	2140±100[35]	1970±100[37]	2060±120[35]

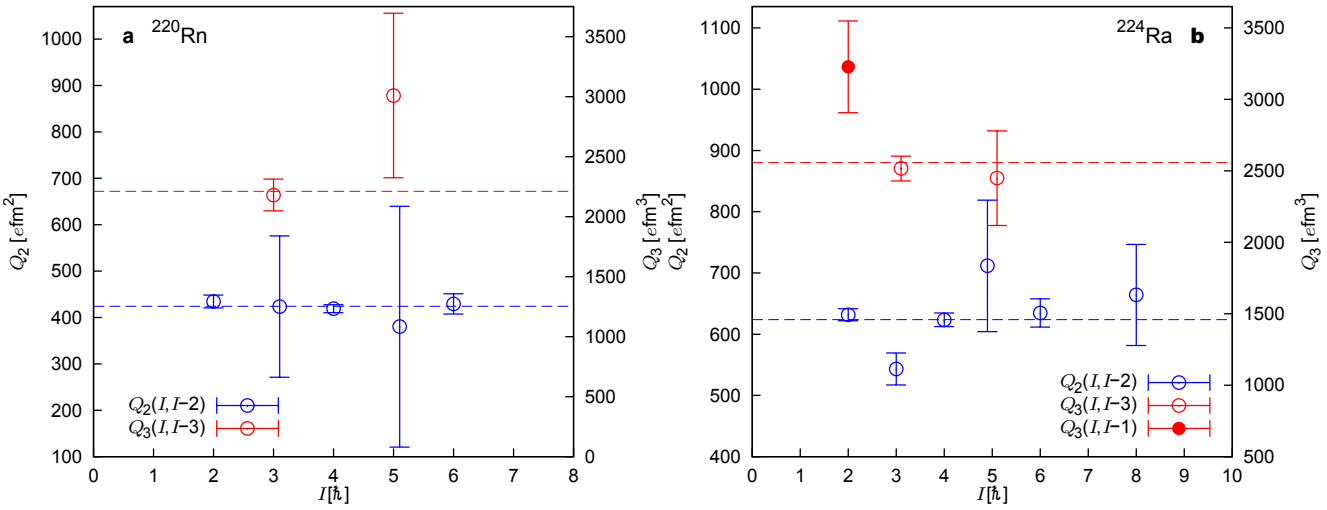

Figure 3. The values of the $E2$ and $E3$ intrinsic moments $Q_\lambda(I,I')$ derived from the matrix elements using the relation $\langle I' \| E_\lambda \| I \rangle = \sqrt{(2I+1)(2\lambda+1)/16\pi}\,(I'0\lambda0 \mid I0)Q_\lambda$ for (a) ^{220}Rn and (b) ^{224}Ra. The dashed lines have the value of the weighted mean for each Q_λ.

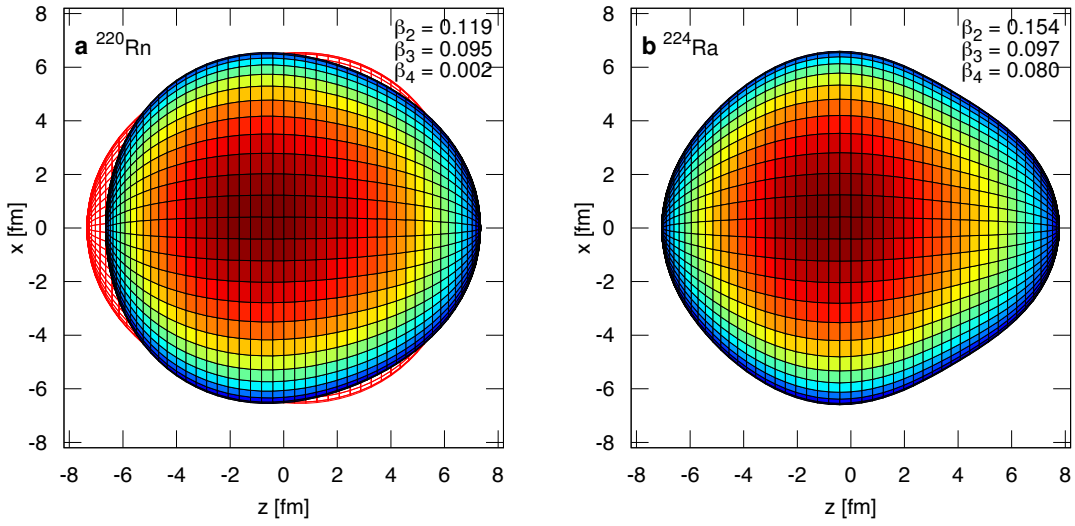

Figure 4. Graphical representation of the shapes of (a) ^{220}Rn and (b) ^{224}Ra. Fig. (a) depicts vibrational motion about symmetry between the surface shown and the red outline, while (b) depicts static deformation in the intrinsic frame. Theoretical values of β_4 are taken from ref. 10. The colour scale, blue to red, represents the y-value of the surface.

The conclusions drawn from the present measurements are also consistent with suggestions from the systematic studies of energy levels[7] (relative alignment of the negative-parity band to the positive-parity band) that the even-even isotopes $^{218\text{-}222}$Rn and ^{220}Ra have vibrational behaviour while $^{222\text{-}228}$Ra have octupole-deformed character (see figures 12 and 13 in ref. 7). For odd-mass ^{219}Ra there is no evidence[40] for parity doubling whereas for ^{221}Ra a parity doublet of states with I=5/2 separated by

103.6 keV has been observed[41]. In the Ba-Nd region with Z~56 and N~88, where the octupole states arise from vibrational coupling to the ground-state band, the evidence for parity doubling of the ground state arising from reflection asymmetry is inconclusive[42,43]. This suggests that the parity doubling condition that leads to enhancement of the Schiff moment[15] is unlikely to be met in ^{219,221}Rn. On the other hand ^{223,225}Ra, having parity doublets separated by ~ 50 keV [21], will have large enhancement of their EDMs.

The values of Q_λ, deduced from the measured transition matrix elements, are plotted in figure 5 as a function of N. The anomalously low value of Q_1 for ^{224}Ra, measured here for the first time, has been noted elsewhere[9,13,47]. The measured Q_1 and Q_2 values are in good agreement with recent theoretical calculations of the generator-coordinate extension of the Gogny Hartree-Fock-Bogoliubov (HFB) self-consistent mean field theory[16], particularly using the D1M parameterisation[44]. However, as remarked earlier, the trend of the experimental data is that the values of Q_3 decrease from a peak near ^{226}Ra with decreasing N (or A), which is in marked contrast to the predictions of the cluster model calculations[17]. It is also at variance with the Gogny mean-field predictions of a maximum for ^{224}Ra [16]. It should be noted, however, that relativistic mean field calculations[14] predict that the maximum value of Q_3 occurs for radium isotopes between A = 226 and 230, depending on the parameterisation, and Skyrme Hartree-Fock calculations[15] predict that ^{226}Ra has the largest octupole deformation, both consistent with our data. We cannot completely eliminate the possibility that there are unobserved couplings from the ground state to higher-lying 3^- states that should be added (without energy weighting) to the observed coupling to the lowest 3^- state. However, in a detailed study of octupole strength in ^{148}Nd [38] where these states lie closer in energy to the lowest state, such couplings were not observed.

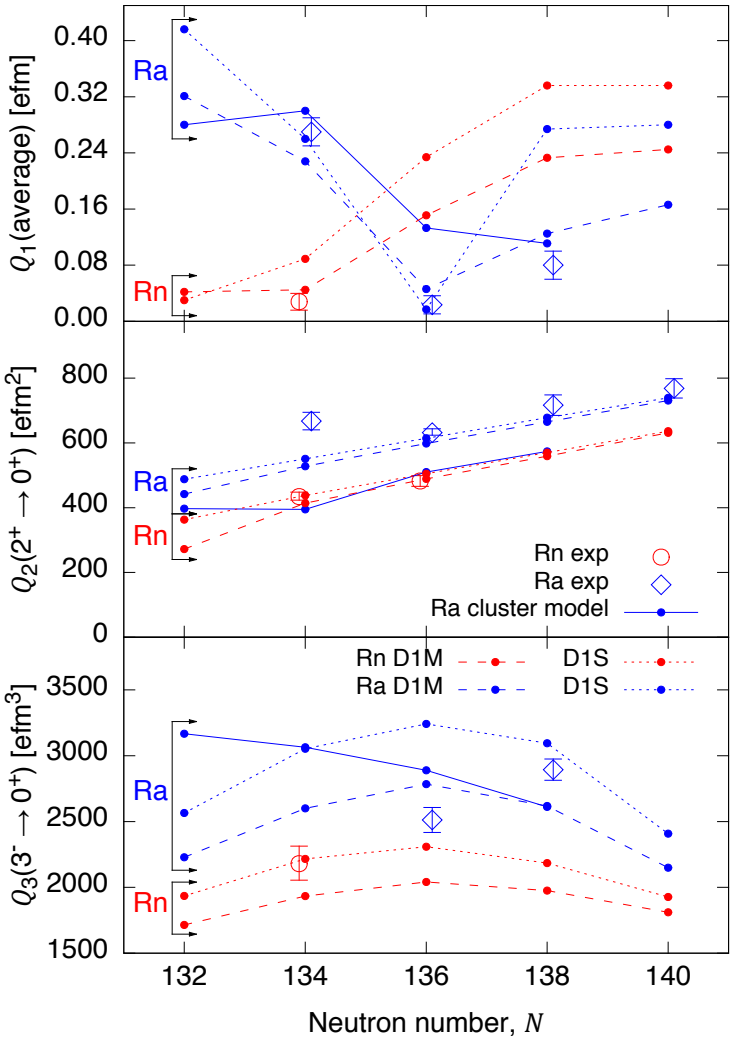

Figure 5. Measured values of Q_λ for the $\lambda \rightarrow 0$ transitions in nuclei as a function of N, except for λ=1, where an average value over the measured spin range ($\leq 5\hbar$) is used. Comparisons are made to the theoretical predictions of a cluster model by Shneidman *et al.*[17] and mean-field calculations (with two different parameterisations[44]) by Robledo and Bertsch[16]. The points are connected by lines as a guide to the eye. The experimental data for ^{220}Rn (N=134) and ^{224}Ra (N=136) are from the present work, other data are taken from refs. 23,45,46. [Please not that the error bars on Q_2 for ^{222}Ra (N=134), ^{222}Rn (N=136), and ^{228}Ra (N=140) have been corrected from those published in doi:10.1038/nature12073.]

We can summarise our findings as follows: we have demonstrated that radioactive beams of heavy nuclei with A~220 can be successfully accelerated with sufficient intensity to measure both even- and odd-order electric-multipole matrix elements with an accuracy of 10% or better. The extracted electric-quadrupole and -octupole moments are consistent with constant values over the range of measured angular momentum. Our data show that ^{220}Rn has weaker octupole collectivity than ^{224}Ra. We conclude that ^{219,221}Rn are likely to have smaller octupole-enhanced EDMs than ^{223,225}Ra. More

favourable Rn candidates may emerge from future studies of the low-lying structure of heavier isotopes. Concerning recent models that are able to predict the $E3$ strength, the trend in octupole deformation extracted from available data reveals detailed differences with some mean field predictions[16] and opposes the trend predicted by the cluster model[17]. These findings should be confirmed by extending studies to other radioactive isotopes in the Rn and Ra chain. It is interesting to note that the Gogny HFB calculations[16] predict that Th and U isotopes with N = 134-136, already known to exhibit the characteristics of a rigid octupole shape[7,48], should have significantly enhanced $E3$ transition strengths (70 Wu); however, the test of this prediction awaits major developments in radioactive beam technology.

METHODS SUMMARY

In our experiments, the ^{220}Rn and ^{224}Ra produced by spallation diffused to the primary target surface and were then ionised ($q=1^+$) in either an enhanced plasma ion-source[49] with a cooled transfer line (Rn) or a tungsten surface ion-source (Ra), accelerated to 30 keV, separated according to A/q, and delivered to a Penning trap, REXTRAP[50], at a rate of around 1.25×10^7 ions/s for ^{220}Rn and 4.4×10^7 ions/s for ^{224}Ra at the entrance. Inside the trap, the singly-charged ions were accumulated and cooled before allowing the ions to escape in bunches at 400 ms intervals into an electron-beam ion source, REXEBIS[50], Here, the ions were confined for 400 ms in a high-density electron beam that stripped more electrons to produce a charge state of 52^+, extracted as 400 μs pulses before being mass-selected again according to A/q, and injected at 2.5 Hz into the REX linear post-accelerator. The level of isobaric impurity (e.g. Fr) in the Ra beam was estimated to be below 1% by observing radioactive decays at the end of the beam line. For Rn, observation of contaminant decays was more difficult because of the small α-decay branching ratios to excited states and only an upper limit of 5% could be obtained.

The GOSIA code performs a least-squares fit to the matrix elements between all known states coupled by electromagnetic operators, which are treated as free parameters. Although the fit is sensitive to the relative $E1/E2$ decay rates, at the beam energies used $E1$ (and $M1$) excitation is negligible and can be ignored. The magnitudes of the values of the starting parameters were chosen to be random, within reasonable limits. The fit was found to be insensitive to many of the matrix elements; these were either fixed or coupled to other matrix elements assuming the validity of the rotational model.

BIBLIOGRAPHY

[1] Pospelov, M. & Ritz, A. Electric dipole moments as probes of new physics. *Annals of Physics* **318**, 119-169 (2005).

[2] Griffith, W. C. *et al.* Improved Limit on the Permanent Electric Dipole Moment of ^{199}Hg. *Phys. Rev. Lett.* **102**, 101601 (2009).

[3] Spevak, V., Auerbach, N. & Flambaum, V. V. Enhanced T-odd, P-odd electromagnetic moments in reflection asymmetric nuclei. *Phys. Rev. C* **56**, 1357–1369 (1997).

[4] Dobaczewski, J. & Engel, J. Nuclear Time-Reversal Violation and the Schiff Moment of ^{225}Ra. *Phys. Rev. Lett.* **94**, 232502 (2005).

[5] Ellis, J., Lee, J. & Pilaftsis, A. Maximal electric dipole moments of nuclei with enhanced Schiff moments. *Journal of High Energy Physics* **2011**, 1–25 (2011).

[6] Guest, J.R. *et al.* Laser Trapping of ^{225}Ra and ^{226}Ra with Repumping by Room-Temperature Blackbody Radiation. *Phys. Rev. Lett.* **98**, 093001 (2007).

[7] Cocks, J. *et al.* Spectroscopy of Rn, Ra and Th isotopes using multi- nucleon transfer reactions.

Nuclear Physics A **645**, 61 – 91 (1999).

[8] Dahlinger, M. *et al.* Alternating parity bands and octupole effects in ^{221}Th and ^{223}Th. *Nuclear Physics A* **484**, 337 – 375 (1988).

[9] Butler, P. A. & Nazarewicz, W. Intrinsic dipole moments in reflection- asymmetric nuclei. *Nuclear Physics A* **533**, 249 – 268 (1991).

[10] Nazarewicz, W. *et al.* Analysis of octupole instability in medium-mass and heavy nuclei. *Nuclear Physics A* **429**, 269 – 295 (1984).

[11] Möller, P. *et al.* Axial and reflection asymmetry of the nuclear ground state. *Atomic Data and Nuclear Data Tables* **94**, 758 - 780 (2008).

[12] Bonche, P., Heenen, P.H., Flocard, H. & Vautherin, D. Self-consistent calculation of the quadrupole-octupole deformation energy surface of ^{222}Ra. *Physics Letters* B **175**, 387 - 391 (1986)

[13] Egido, J. & Robledo, L. Microscopic study of the octupole degree of freedom in the radium and thorium isotopes with Gogny forces. *Nuclear Physics A* **494**, 85 – 101 (1989).

[14] Rutz, K., Maruhn, J.A., Reinhard, P.-G. & Greiner, W. Fission barriers and asymmetric ground states in the relativistic mean-field theory. *Nuclear Physics* A **590**, 680 - 702 (1995).

[15] Engel, J., Bender, M., Dobaczewski, J., Jesus, J. H. d. & Olbratowski, P. Time-reversal violating Schiff moment of ^{225}Ra. *Phys. Rev. C* **68**, 025501 (2003).

[16] Robledo, L. M. & Bertsch, G. F. Global systematics of octupole excitations in even-even nuclei. *Phys. Rev. C* **84**, 054302 (2011).

[17] Shneidman, T. M., Adamian, G. G., Antonenko, N. V., Jolos, R. V. & Scheid, W. Cluster interpretation of properties of alternating parity bands in heavy nuclei. *Phys. Rev. C* **67**, 014313 (2003).

[18] Buck, B., Merchant, A. C. & Perez, S. M. Negative parity bands in even–even isotopes of Ra, Th, U and Pu. *Journal of Physics G: Nuclear and Particle Physics* **35**, 085101 (2008).

[19] Zamfir, N. V. & Kusnezov, D. Octupole correlations in the transitional actinides and the spdf interacting boson model. *Phys. Rev. C* **63**, 054306 (2001).

[20] Frauendorf, S. Heart-shaped nuclei: Condensation of rotational-aligned octupole phonons. *Phys. Rev. C* **77**, 021304 (2008).

[21] Butler, P. A. & Nazarewicz, W. Intrinsic reflection asymmetry in atomic nuclei. *Rev. Mod. Phys.* **68**, 349 – 421 (1996).

[22] Robledo, L. M. & Bertsch, G. F., Electromagnetic transition strengths in soft deformed nuclei. *Phys. Rev. C* **86**, 054306 (2012).

[23] Wollersheim, H. J. *et al.* Coulomb excitation of ^{226}Ra. *Nuclear Physics A* **556**, 261 – 280 (1993).

[24] Voulot, D. *et al.* Radioactive beams at REX–ISOLDE: Present status and latest developments. *Nuclear Instruments and Methods in Physics Research Section B: Beam Interactions with Materials and Atoms* **266**, 4103 – 4107 (2008).

[25] Eberth, J. *et al.* MINIBALL A Ge detector array for radioactive ion beam facilities. *Progress in Particle and Nuclear Physics* **46**, 389 – 398 (2001).

[26] Ostrowski, A. *et al.* CD: A double sided silicon strip detector for radioactive nuclear beam experiments. *Nuclear Instruments and Methods in Physics Research Section A: Accelerators, Spectrometers, Detectors and Associated Equipment* **480**, 448 – 455 (2002).

[27] Bell, R. E., Bjornholm, S. & Severiens, J. C. Half Lives of First Excited States of Even Nuclei of Fm, Ra, Th, U, and Pu. *Kgl. Danske Vid. Selsk. Mat.-Fys. Medd.* **12**, 32 (1960).

[28] Neal, W. R. & Kraner, H. W. Mean Lives of Excited Rotational States of Heavy Even-Even

Nuclei. *Phys. Rev.* **137**, B1164 – B1174 (1965).

[29] Liang, C. F., Paris, P., Ruchowska, E. & Briancon, C. A new isotope $_{85}^{220}At_{135}$. *Journal of Physics G: Nuclear and Particle Physics* **15**, L31 (1989).

[30] Artna-Cohen, A. Nuclear Data Sheets for A = 224. *Nuclear Data Sheets* **80**, 227 – 262 (1997).

[31] Cline, D. Quadrupole and octupole shapes in nuclei. *Nuclear Physics A* **557**, 615 – 634 (1993).

[32] Nazarewicz, W. and Tabor, S.L. Octupole shapes and shape changes at high spins in the Z ~58, N ~88 nuclei. *Phys. Rev. C* **45**, 2226-2237 (1992).

[33] Martin, M.J. Nuclear Data Sheets for A = 208. *Nuclear Data Sheets* **108**, 1583 – 1806 (2007).

[34] Bemis, C. E. *et al.* E2 and E4 Transition Moments and Equilibrium Deformations in the Actinide Nuclei. *Phys. Rev. C* **8**, 1466 – 1480 (1973).

[35] McGowan, F. K. *et al.* Coulomb excitation of vibrational-like states in the even-A actinide nuclei. *Phys. Rev. C* **10**, 1146 – 1155 (1974).

[36] Baktash, C. & Saladin, J. X. Determination of E2 and E4 transition moments in ^{232}Th. *Phys. Rev. C* **10**, 1136 – 1139 (1974).

[37] McGowan, F. & Milner, W. Coulomb excitation of states in ^{232}Th. *Nuclear Physics A* **562**, 241 – 259 (1993).

[38] Ibbotson, R. W. *et al.* Quadrupole and octupole collectivity in ^{148}Nd. *Nuclear Physics A* **619**, 213 – 240 (1997).

[39] Leander, G. A. & Chen, Y. S. Reflection-asymmetric rotor model of odd A ~ 219–229 nuclei. *Phys. Rev. C* **37**, 2744 – 2778 (1988).

[40] Riley, L. A. *et al.* Conversion electron-γ coincidences and intrinsic reflection asymmetry in ^{219}Ra. *Phys. Rev. C* **62**, 021301 (2000).

[41] Ackermann, B. *et al.* Level structure of ^{217}Rn and ^{221}Ra investigated in the alpha-decay ^{225}Th → ^{221}Ra → ^{217}Rn. *Z. Phys. A* **332**, 375 – 381 (1989).

[42] Nosek, D., Sheline, R.K., Sood, P.C. & Kvasil, J., Microscopic structures of parity doublets in the ^{151}Pm, ^{153}Eu and ^{155}Eu nuclei. *Z. Phys. A* **344**, 277 – 283 (1993).

[43] Rząca-Urban, T. *et al.* Reflection symmetry of the near-yrast excitations in ^{145}Ba. *Phys. Rev. C* **86**, 044324 (2012).

[44] Goriely, S., Hilaire, S., Girod, M. & Péru, S., First Gogny-Hartree-Fock-Bogoliubov Nuclear Mass Model. *Phys. Rev. Letts.* **102**, 242501 (2009).

[45] Singh, S., Jain, A. & Tuli, J. K. Nuclear Data Sheets for A = 222. *Nuclear Data Sheets* **112**, 2851 – 2886 (2011).

[46] Artna-Cohen, A. Nuclear Data Sheets for A = 228. *Nuclear Data Sheets* **80**, 723 – 786 (1997).

[47] Poynter, R. J. *et al.* Observation of unexpectedly small E1 moments in ^{224}Ra. *Phys. Lett. B* **232**, 447 – 451 (1989).

[48] Greenlees, P. T. *et al.* First observation of excited states in ^{226}U. *Journal of Physics G: Nuclear and Particle Physics* **24**, L63 (1998).

[49] Penescu, L., Catherall, R., Lettry, J. & Stora, T. Development of high efficiency Versatile Arc Discharge Ion Source at CERN ISOLDE. *Review of Scientific Instruments* **81**, 02A906 (2010).

[50] Wolf, B. H. *et al.* First radioactive ions charge bred in REXEBIS at the REX-ISOLDE accelerator. *Nuclear Instrum. and Meth. in Physics Research B* **204**, 428 – 432 (2003)

Acknowledgments The support of the ISOLDE Collaboration and technical teams is acknowledged. This work was supported by the following Research Councils: STFC (UK), BMBF(Germany; 05P12RDCIA, 06DA9036I, 06KY9136I and 06KY205I), HIC for FAIR (Germany), FWO-Vlaanderen (Belgium), Belgian Science Policy Office (IAP-BriX network P7/12), Academy of Finland (contract number 131665), DOE (US; DE-AC52-07NA27344 and DE-FG02-04ER41331), NSF (US), MICINN (Spain; FPA2009-08958 and FIS2009-07277), Consolider-Ingenio 2010 Programmes (Spain; CPAN CSD2007-00042 and MULTIDARK CSD2009-00064), Polish Ministry for Science and Higher Education (Grant no. 589/N-G-POOL/2009/0), EC via I3-EURONS (FP6 contract no. RII3-CT-2004-506065), MC Fellowship scheme (FP7 contract PIEF-GA-2008-219175) and IA-ENSAR (FP7 contract 262010).

Author Contributions Instrument set up: M Albers, C Bauer, A Blazhev, T Davinson, H De Witte, LP Gaffney, J Konki, J Pakarinen, P Reiter, M Seidlitz, B Siebeck, M Vermeulen, N Warr; DAQ & on-line analysis: A Blazhev, LP Gaffney, R Lutter, N Warr; Data analysis & interpretation: LP Gaffney, PA Butler, D Cline, A Hayes, M Scheck, M Zielinska; REX development and setup: F Wenander, D Voulot, J. Cederkäll; Primary Target: T. Stora; Preparation of manuscript: PA Butler, LP Gaffney, T Chupp, A Blazhev, DG Jenkins, Th. Kröll, J Pakarinen, P Reiter, M Scheck, P Van Duppen, N Warr; Theoretical interpretation: L.M. Robledo. All authors except LM Robledo took part in the experiments

Author Information Reprints and permissions information is available at www.nature.com/reprints. The authors declare no competing financial interests. Readers are welcome to comment on the online version of this article at www.nature.com/nature. Correspondence and requests for materials should be addressed to Peter Butler (peter.butler@liverpool.ac.uk)